Cell. Mol. Life Sci. (2013) 70:105–120
DOI 10.1007/s00018-012-1059-5

Cellular and Molecular Life Sciences

RESEARCH ARTICLE

GSK3 and β-catenin determines functional expression of sodium channels at the axon initial segment

Mónica Tapia · Ana Del Puerto · Alberto Puime · Diana Sánchez-Ponce · Laure Fronzaroli-Molinieres · Noemí Pallas-Bazarra · Edmond Carlier · Pierre Giraud · Dominique Debanne · Francisco Wandosell · Juan José Garrido

Received: 16 January 2012 / Revised: 21 May 2012 / Accepted: 12 June 2012 / Published online: 5 July 2012

Abstract Neuronal action potentials are generated through voltage-gated sodium channels, which are tethered by ankyrinG at the membrane of the axon initial segment (AIS). Despite the importance of the AIS in the control of neuronal excitability, the cellular and molecular mechanisms regulating sodium channel expression at the AIS remain elusive. Our results show that GSK3α/β and β-catenin phosphorylated by GSK3 (S33/37/T41) are localized at the AIS and are new components of this essential neuronal domain. Pharmacological inhibition of GSK3 or β-catenin knockdown with shRNAs decreased the levels of phosphorylated-β-catenin, ankyrinG, and voltage-gated sodium channels at the AIS, both "in vitro" and "in vivo", therefore diminishing neuronal excitability as evaluated via sodium current amplitude and action potential number. Thus, our results suggest a mechanism for the modulation of neuronal excitability through the control of sodium channel density by GSK3 and β-catenin at the AIS.

Keywords β-catenin · Axon initial segment · GSK3 · AnkyrinG · Sodium channels

Electronic supplementary material The online version of this article (doi:10.1007/s00018-012-1059-5) contains supplementary material, which is available to authorized users.

M. Tapia · A. Del Puerto · D. Sánchez-Ponce · N. Pallas-Bazarra · J. J. Garrido (✉)
Department of Cellular, Molecular and Developmental Neurobiology, Instituto Cajal, CSIC, Avenida Doctor Arce, Madrid 28002, Spain
e-mail: jjgarrido@cajal.csic.es

M. Tapia · A. Del Puerto · D. Sánchez-Ponce · N. Pallas-Bazarra · F. Wandosell · J. J. Garrido
Centro de Investigación Biomédica en Red sobre Enfermedades Neurodegenerativas (CIBERNED), Madrid, Spain

A. Puime
Departamento de Anatomía Patológica, Capio Fundación Jiménez Díaz, Madrid 28040, Spain

L. Fronzaroli-Molinieres · E. Carlier · P. Giraud · D. Debanne
INSERM U1072, Marseille 13344, France

L. Fronzaroli-Molinieres · E. Carlier · P. Giraud · D. Debanne
Aix-Marseille University, U1072, Marseille 13344, France

Introduction

After axonal specification, the development of the axon initial segment (AIS), characterized by a high density of voltage-gated Na^+ and K^+ channels, is critical in initiating and modulating action potentials [1, 2]. These ion channels and other AIS membrane proteins, such as neurofascin, are tethered by intracellular proteins, such as ankyrinG or PSD-93 [3–6]. The cytoskeleton of the AIS is characterized by ultrastructural features such as dense F-actin microfilaments or fasciculated microtubules, which are resistant to detergent extraction and display a higher degree of tubulin acetylation and detyrosination [7–11]. These characteristics confer on the AIS the ability to act as a barrier to membrane diffusion [11] and to cytoplasmic traffic [12, 13]. However, the signaling pathways regulating AIS functional maintenance remain largely unknown. AnkyrinG is necessary for maintaining the AIS [14] and seems to be essential for maintaining microtubule properties at the AIS [15] like CK2 and HDAC6 [9, 10].

GSK3 is a key kinase downstream of multiple regulatory pathways, and regulates microtubule dynamics, neuronal differentiation, axon guidance, axonal protein transport, as well as ion channel activity [16–19]. In addition to its function in regulating microtubule dynamics, GSK3 can

phosphorylate proteins detected at the AIS, such as the GABA receptor scaffolding protein gephyrin [20]. GSK3 also has an important function in β-catenin regulation, a multifaceted protein involved among other functions in cell structure.

β-catenin has been implicated in adhesion or transcription [21]. The regulation of these different functions is complex and controlled by differential phosphorylation of β-catenin or distinct protein interactions in different subcellular compartments. For example, a minor pool of β-catenin is phosphorylated by GSK3β at S33, S37, and T41 [22], ubiquitinated after interaction with βTrCP E3 ligase and degraded by the proteasome [23]. However, recent studies have shown that β-catenin-pS33/37/T41 may not only be involved in degradation but also in determining signaling functions [24, 25]. In epithelial cells, β-catenin phosphorylated by GSK3 is localized at tight junctions 24, associated with APC at the leading edge of migrating cells [24], and is involved in microtubule re-growth at the centrosome [26]. β-catenin also forms a complex with N-cadherin, dynein/dynactin/p150, and the EB1 microtubule plus end protein at adherent junctions [27]. Besides cadherins, many β-catenin-binding proteins belong to the family of microtubule-related proteins [28]. In neurons, β-catenin has been reported to be a critical mediator of dendritic morphogenesis [29] and axonal growth [30]. β-catenin knock-out mice dye in early embryonic development [31] and several conditional β-catenin knock-out have significant impaired craneo-encephalic development or cortical and hippocampal development [32]. Moreover, β-catenin is also a binding partner of APC, a microtubule-binding protein and can regulate the level of APC clusters in neurite tips [33]. β-catenin also interacts with Ca^{2+}-activated K^+ channels in presynaptic active zones [34].

In the present study, we found that β-catenin phosphorylated at S33/S37/T41 is progressively accumulated at the AIS during neuronal development. β-catenin-pS33/37/T41 tethered at the AIS shares the same characteristics as other AIS proteins, and its concentration at the AIS depends on the microtubule cytoskeleton. Moreover, we describe that GSK3 is localized at the AIS, and its inhibition, as well as the reduction of β-catenin expression by specific shRNAs, affects the normal clustering of ankyrinG and voltage-gated sodium channels at the AIS and reduces neuronal excitability. In conclusion, our results show that β-catenin and GSK3 play a role during functional maturation of the AIS.

Materials and methods

Cell culture

All protocols were approved by the institutional animal care and use committee following the guidelines of the Council of Europe Convention ETS123, recently revised as indicated in the Directive 86/609/EEC. Hippocampal and cortical neurons were prepared as previously described [35]. The cells were plated on polylysine-coated coverslips (1 mg/ml) at a density of 7,500 cells/cm^2. 5 μM 1-β-D-arabinofuranosylcytosine (AraC) was added after 2 days in culture. For biochemical experiments, cortical neurons were plated at a density of 100,000 cells/cm^2, and cultured for 48 h. For the culture of neurons beyond 6 DIV, neurons were plated at a density of 5,000 cells/cm^2 and transferred to dishes containing astrocytes. Primary hippocampal neurons were nucleofected using the Amaxa nucleofector kit for primary mammalian neural cells (Amaxa Bioscience) according to the manufacturer's instructions. Nucleofection was performed using 3 μg total DNA and 3×10^6 cells for each nucleofection. Nucleofection efficiency was around 15 % of neurons, based on RFP protein expression.

Murine neuroblastoma N2a were originally obtained from the American Type Cell Culture (Neuro-2A, Reference: CCL131) and were grown at 37 °C in 7 % CO_2, in DMEM supplemented with 10 % fetal bovine serum (FBS, Invitrogen) and 2 mM glutamine. N2a cells were transfected using Lipofectamine 2000 (Invitrogen) according to the manufacturer's instructions. Transfections were performed with 9 μl Lipofectamine 2000 and 3 μg plasmid DNA.

Reagents and plasmids

Interference RNA plasmids were obtained from Origene. Two different shRNA sequences against β-catenin and a scrambled shRNA were used, inserted into the pRFP-C-RS vector, which expresses the red fluorescent protein. An shRNA-AnkyrinG and scrambled sequence in pGFP-V-RS were used for ankyrinG [9]. Lithium chloride (LiCl), myo-inositol phosphate, Trichostatin A (TSA), and Nocodazole were from Sigma. GSK3 inhibitor X and GSK3 inhibitor AR-A014418 were from Calbiochem.

Immunocytochemistry

Hippocampal neurons were fixed in 4 % paraformaldehyde for 20 min. In some experiments, 15-DIV neurons were then treated with or without TSA for 48 h, and washed in phosphate buffer before extracting the cells with 0.5 % Triton X-100 in cytoskeletal buffer (2 mM $MgCl_2$, 10 mM EGTA, 60 mM Pipes pH 7.0) for 10 min at 37 °C, modified from previous work [11]. After extraction, the neurons were rinsed and fixed in PFA 4 %. For immunodetection, the coverslips were treated for 10 min with 50 mM NH_4Cl and incubated in blocking buffer (0.22 % gelatin, 0.1 % Triton X-100 in PBS) for 30 min. Primary antibodies were

incubated for 1 h at room temperature in blocking buffer. The primary antibodies used were: mouse anti-acetylated-α-tubulin (1:2,000), mouse anti-tyrosinated-α-tubulin (1:2,000), mouse anti-MAP2 (1:400) and mouse anti-PanNaCh (1:75), mouse anti-α-tubulin (1:100) from Sigma; mouse anti-tau-1 (1:1,000), and rabbit anti-MAP2 (1:500) from Chemicon; mouse anti-ankyrinG (1:100) from NeuroMab; rabbit anti-pS33/S37T41-β-catenin (1:250), rabbit anti-pS45-β-catenin (1:200) and rabbit anti-pS32-IκBα (1:250, 14D4) from Cell Signaling; mouse anti-β-catenin (1:500), mouse anti-N-cadherin (1:200) and mouse anti-EB1 (1:100) from BD Transduction, mouse anti-GSK3α/β (1:1000) from Biosource (Life Technologies); mouse anti-APC (1:150) from Millipore; rabbit anti-βIII tubulin (1:1,000) from Covance; rabbit anti-α-tubulin was kindly provided by Dr. Arevalo lab (Instituto Cajal), and chicken anti-MAP2 (1:10,000) from Abcam. The secondary antibodies used were a donkey anti-mouse or anti-rabbit Alexa-Fluor-488, 594 or 647 (1:500). F-actin was stained using Alexa-Fluor-594-conjugated Phalloidin (1:100). Nuclei were stained using TOPRO.

Images were acquired on a vertical Axioskop-2plus microscope (Zeiss) or a confocal microscope (LSM510, Zeiss) under the same conditions to compare intensities. Analysis of axon length and fluorescence intensities was performed with the NeuronJ and ImageJ software tools. Images were prepared for presentation using the Adobe CS3 software.

Immunohistochemistry

Brains from E18 embryos or P0, P5, and P12 mice were fixed overnight in 4 % paraformaldehyde in 0.1 M phosphate buffer (PB) pH 7.2, cryoprotected in 30 % sucrose and frozen in Tissue-Tek mounting medium (Electron Microscopy Sciences). Brain sections (30 μm) were obtained on a cryostat and collected in PB. The sections were permeabilized for 1 h in 0.1 M PB containing 0.5 % Triton X-100 and 10 % horse serum (GIBCO) and then incubated overnight at room temperature in the same solution containing rabbit anti-pS33/37T41-β-catenin (1:50) and mouse anti-ankyrinG (1:200) antibodies. Secondary antibodies were incubated for 1 h at room temperature. The samples were washed in PB and mounted on slides with Fluoromount-G. Some sections (5 μm) were stained with Giemsa (Merck).

Western-blot analysis

Protein samples were prepared from high-density cortical neuron cultures and murine neuroblastoma N2a cells. The cells were lysed and homogenized in a buffer containing 20 mM HEPES (pH 7.4), 100 mM NaCl, 100 mM NaF, 1 % Triton X-100, 1 mM sodium orthovanadate, 10 mM EDTA and Complete inhibitor protease cocktail (Roche Diagnostics). The proteins were then separated on 8 % SDS-PAGE gels and transferred to nitrocellulose membranes. The membranes were incubated overnight at 4 °C with primary antibodies in blocking solution (PBS, 0.2 % Tween, 5 % non-fat milk or 10 % FBS). The antibodies used to probe the membranes were mouse anti-β-actin (1:5,000, Sigma); anti-β-catenin (1:800, BD Transduction); rabbit anti-pS33/S37T41-β-catenin (1:500) and GAPDH (1:2,000, Cell Signaling). Secondary antibodies were from Amersham. Antibody binding was then visualized by ECL (Amersham) and densitometry was performed with an imaging densitometer (GS-800, Bio-Rad).

Mouse brain slice cultures, plasmid GeneGun delivery, and electrophysiological recording

Slice cultures containing the hippocampus and entorhinal cortex were obtained from post-natal day 8 mice as previously reported [36]. Slices (300–350 μm) were cut in sucrose-based slicing solution (280 mM sucrose, 26 mM $NaHCO_3$, 1.3 mM KCl, 1 mM $CaCl_2$, 10 mM $MgCl_2$, 11 mM D-glucose, 50 mM phenol red, and 2 mM kynurenate) and were maintained for 1 h at room temperature in oxygenated (95 % O_2/5 % CO_2) standard artificial ACSF (125 mM NaCl, 2.5 mM KCl, 0.8 mM NaH_2PO_4, 26 mM $NaHCO_3$, 3 mM $CaCl_2$, 2 mM $MgCl_2$, 50 mM phenol red, and 11 mM D-glucose). Each slice was placed on 20-mm latex membranes (Millicell) inserted into 35-mm Petri dishes containing 1 ml of culture medium (25 ml MEM, 12.5 ml HBSS, 12.5 ml horse serum, 0.5 ml penicillin/streptomycin, 0.8 ml glucose solution (1 M), 0.1 ml ascorbic acid solution (1 mg/ml), 0.4 ml HEPES (1 M), 0.5 ml B27, and 8.95 ml water) and maintained for up to 8–9 days in an incubator at 34 °C, 95 % O_2–5 % CO_2. To arrest glial proliferation, 5 μM Ara-C was added to the culture medium starting at 3 days in vitro. The GSK-3 inhibitor, AR-A014418 (20 μM), was added to cultured slices at 1 day in vitro and kept for 7 days. β-catenin shRNAs plasmids were delivered to brain slices using the Helyos gene-gun system (Bio-Rad) according to the manufacturer's instructions. Briefly, gold particles coated with scrambled or β-catenin shRNA were introduced into cells employing a high-velocity stream of helium (120 dpi) at 2 days in vitro and the slices were maintained for up to 7 days.

Whole-cell patch clamp recordings were obtained from CA3 or L5 pyramidal neurons. The external solution contained (mM): 125 NaCl, 26 $NaHCO_3$, 3 $CaCl_2$, 2.5 KCL, 2 $MgCl_2$, 0.8 NaH_2PO_4, and 10 D-glucose, and was equilibrated with 95 % O_2–CO_2. Patch pipettes (5–10 MΩ) were filled with a solution containing (mM): 120 potassium

gluconate, 20 KCl, 0.5 EGTA, 10 HEPES, 2 Na_2ATP, 0.3 NaGTP and 2 MgCl2, pH 7.4. Recordings were made at 29 °C. The voltage and current signals were low-pass filtered (3 kHz) and acquisition of sequences (500–1,500 ms) was performed at a frequency of 0.1 Hz with P-clamp 8 or 10 (Axon Instruments). Sodium currents were evoked by a voltage step (50 ms) from −80 to −20 mV. The capacitive and leak components of the evoked current were subtracted with a conventional P/4 protocol. Intrinsic neuronal excitability was monitored with depolarizing current pulses (1 s) of increasing amplitude (from +10/+ 500 pA).

Statistical analysis

All experiments were repeated at least three times and the results are presented as the mean and standard error of the mean (SEM) or standard deviation of the mean (SD) as indicated in figure legends. Statistical differences between experimental conditions were analyzed by *t* test or paired *t* test using the Sigmaplot 11.0 software.

Results

GSK3 phosphorylated β-catenin is enriched at the axon initial segment

Previous studies have shown a relationship between GSK3 phosphorylated β-catenin (S33/37/T41) and cell polarity [24, 25]. To test this hypothesis in neurons, we first studied the location of β-catenin-pS33/37/T41 in different developmental stages of hippocampal neurons using a phospho-specific antibody raised against β-catenin phosphorylated on the N-terminal Ser 33, Ser 37, and Thr 41, which specificity has been tested in a β-catenin knockout mouse at early developmental stages [37] and a β-catenin antibody that recognizes the C-terminal region. The specificity of phosphorylated β-catenin antibody was further confirmed by suppression of β-catenin expression with nucleofected β-catenin shRNAs (Supplementary Fig. 1) and β-catenin shRNAs expression resulted in the absence of β-catenin and β-catenin-pS33/37/T41 staining. At an early stage (24 h), we found β-catenin-pS33/37/T41 concentrated at soma (Fig. 1a) and at a higher levels at the centrosome of hippocampal neurons, as previously described in epithelial cells and neural progenitors (Supplementary Fig. 2; [26, 37]). β-catenin-pS33/37/T41 staining was also located all along the neurites, co-localizing with tubulin staining, while β-catenin antibody mainly stained the leading edge of neurites, colocalized with the F-actin-rich region (Fig. 1a). Following axonal elongation at 48 h, β-catenin-pS33/37/T41 was mainly polarized to the axon, even though a lower level of phospho-β-catenin still remained in the other neurites (Fig. 1b).

We then examined the expression of β-catenin-pS33/37/T41 at later stages of development. Interestingly, 3, 6, or 21-DIV (days in vitro) hippocampal neurons showed β-catenin-pS33/37/T41 staining concentrated at the AIS (Fig. 1c–e). AISs were identified by ankyrinG, voltage-gated sodium channel or the AIS marker 14D4 staining. The percentage of ankyrinG-positive AISs with colocalized β-catenin-pS33/37/T41 staining increased from 43 ± 7 % at 3 DIV to 82 ± 1 % at 7 DIV (Fig. 1f), and the same staining was maintained in older neurons (Fig. 1e). Fluorescence intensity along dendrites, soma, and axon at different developmental stages was quantified to confirm a higher AIS intensity fluorescence of β-catenin-pS33/37/T41 than in other regions of the neuron (Supplementary Fig. 3). On the other hand, β-catenin antibody stained dendrites and axons, and was also observed at the AIS (Fig. 1g). The differences in β-catenin antibodies staining may be due to molecular interactions in each neuronal region and antibody accessibility to the different epitopes. In fact, β-catenin phosphorylated at serine 45 is not located at the AIS, and is enriched in the nucleus of hippocampal neurons (Supplementary Fig. 4). This spatial uncoupling of β-catenin phosphorylation has been previously observed in epithelial cells [25]. Finally, treatment of 6-DIV hippocampal neurons with the proteasome inhibitor MG132 (50 nM) increased β-catenin-pS33/37/T41 levels at the soma, but did not change β-catenin-pS33/37/T41 levels at the AIS (Supplementary Fig. 5), suggesting that β-catenin-pS33/37/T41 may be protected by other proteins at the AIS.

We next analyzed the expression of β-catenin-pS33/37/T41 in developing mice brains from E18 to P12 (Fig. 2). Brain sections were stained using the polyclonal anti-β-catenin-pS33/37/T41 antibody and a monoclonal anti-ankyrinG antibody to identify axon initial segments (see "Materials and methods"). At E17–18, we did not detect any localization of β-catenin-pS33/37/T41 (data not shown) and AISs were not yet formed [38]. Some scattered AISs were detected at P0 (Fig. 2a), and at P5 and P12 β-catenin-pS33/37/T41 staining of AISs was progressively detected throughout the cortical plate to layer VI colocalized with ankyrinG staining (Fig. 2b, d) and in the pyramidal cell layer of CA1, CA2, and CA3 of the hippocampus (Fig. 2c).

β-catenin-pS33/37/T41 tethering at the AIS depends on AnkyrinG and AIS microtubules

In order to identify a molecular partner of phospho-β-catenin at the AIS, we first checked the localization of two known β-catenin-interacting proteins, N-cadherin and APC, which play an important role in adhesion complex and microtubule interactions, respectively. As shown in Supplementary Fig. 6, neither N-cadherin nor APC were identified at the AIS in 6-DIV neurons.

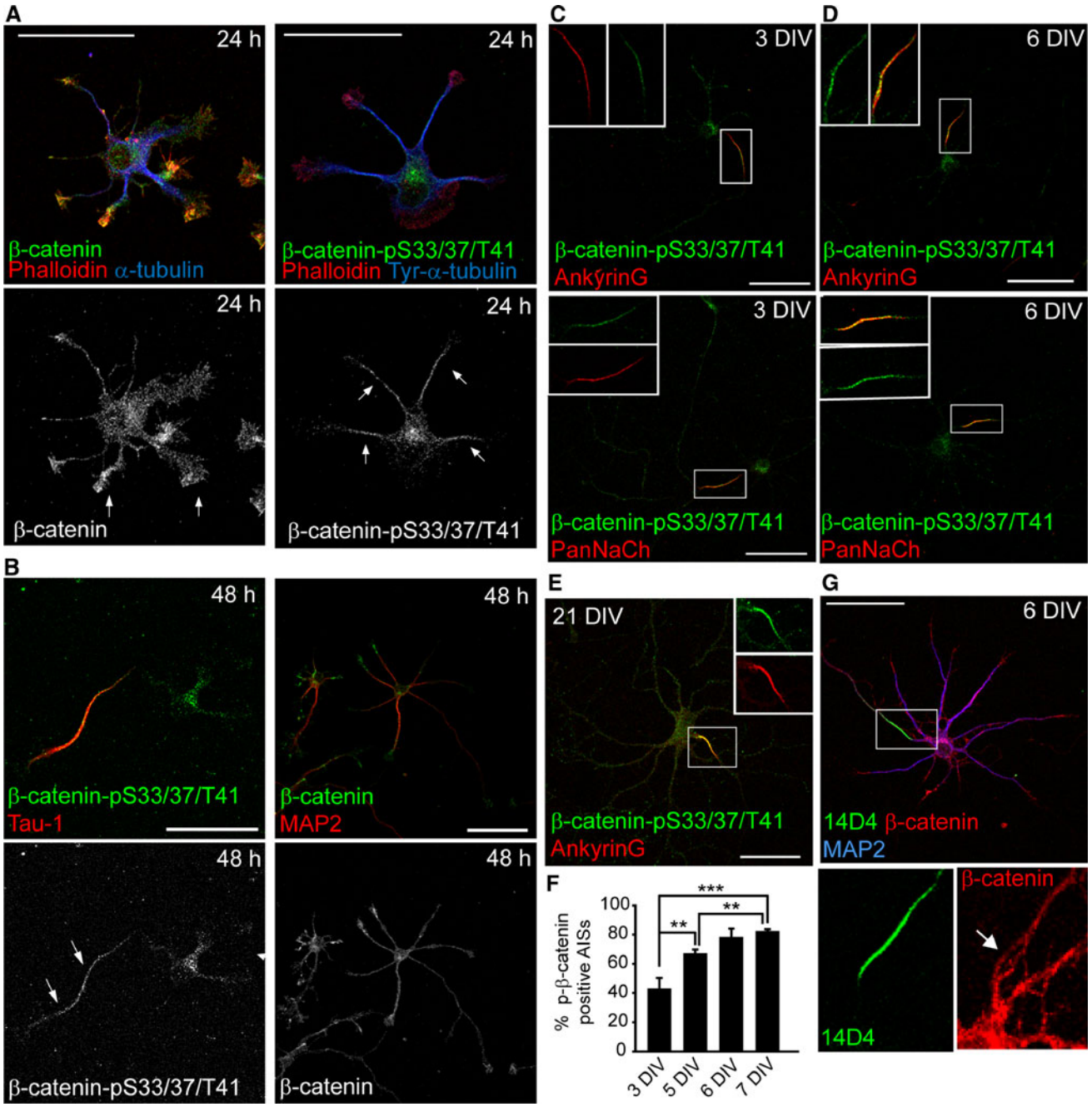

Fig. 1 β-catenin-pS33/37/T41 is concentrated at the axon initial segment in cultured hippocampal neurons. **a** Hippocampal neurons cultured for 24 h were stained for F-actin (*red*) and antibodies against α-tubulin (*blue*) and β-catenin (*green*) in *left panels*, and tyrosinated-α-tubulin (*blue*) and pS33/37T41-β-catenin (*green*) in *right panels*. *Arrows* indicate higher β-catenin intensity fluorescence at the growth cone in *left panels*, while in *right panels arrows* indicate a tubulin-rich zone with high-intensity fluorescence of pS33/37T41-β-catenin. Note the position of centrosome in neurons labeled with pS33/37T41-β-catenin antibody in the *right panel*. **b** Hippocampal neurons cultured for 48 h were stained with pS33/37T41-β-catenin or β-catenin (*green*) and with tau-1 (axon) or MAP2 (dendrites) antibodies (*red*). *Arrows* indicate the axon (**c**, **d**) 3-DIV and 6-DIV hippocampal neurons were stained with ankyrinG or PanNaCh (*red*) and pS33/37T41-β-catenin (*green*) antibodies. Both proteins are concentrated at the AIS region. *Insets* show enlarged views of overlapping β-catenin-pS33/37/T41 and AnkyrinG or PanNaCh staining at the AIS. **e** 21-DIV neurons stained with antibodies against AnkyrinG (*red*) and β-catenin-pS33/37/T41 (*green*). *Box* shows an amplification of the indicated axon initial segment. **f** Percentage of neurons that show β-catenin-pS33/37/T41 concentrated at the AIS relative to ankyrinG-positive AISs during neuronal differentiation. The *graphs* represent the mean of three independent experiments (500 neurons/experimental condition in each experiment). $^{**}p < 0.01$, $^{***}p < 0.001$, *t* test. **g** Triple immunostaining with β-catenin (*red*), 14D4 antibody (*green*), and MAP2 (*blue*) in 6-DIV neurons. Magnifications show β-catenin staining at the AIS recognized by the 14D4 antibody staining at the AIS. *Scale bar* 50 μm

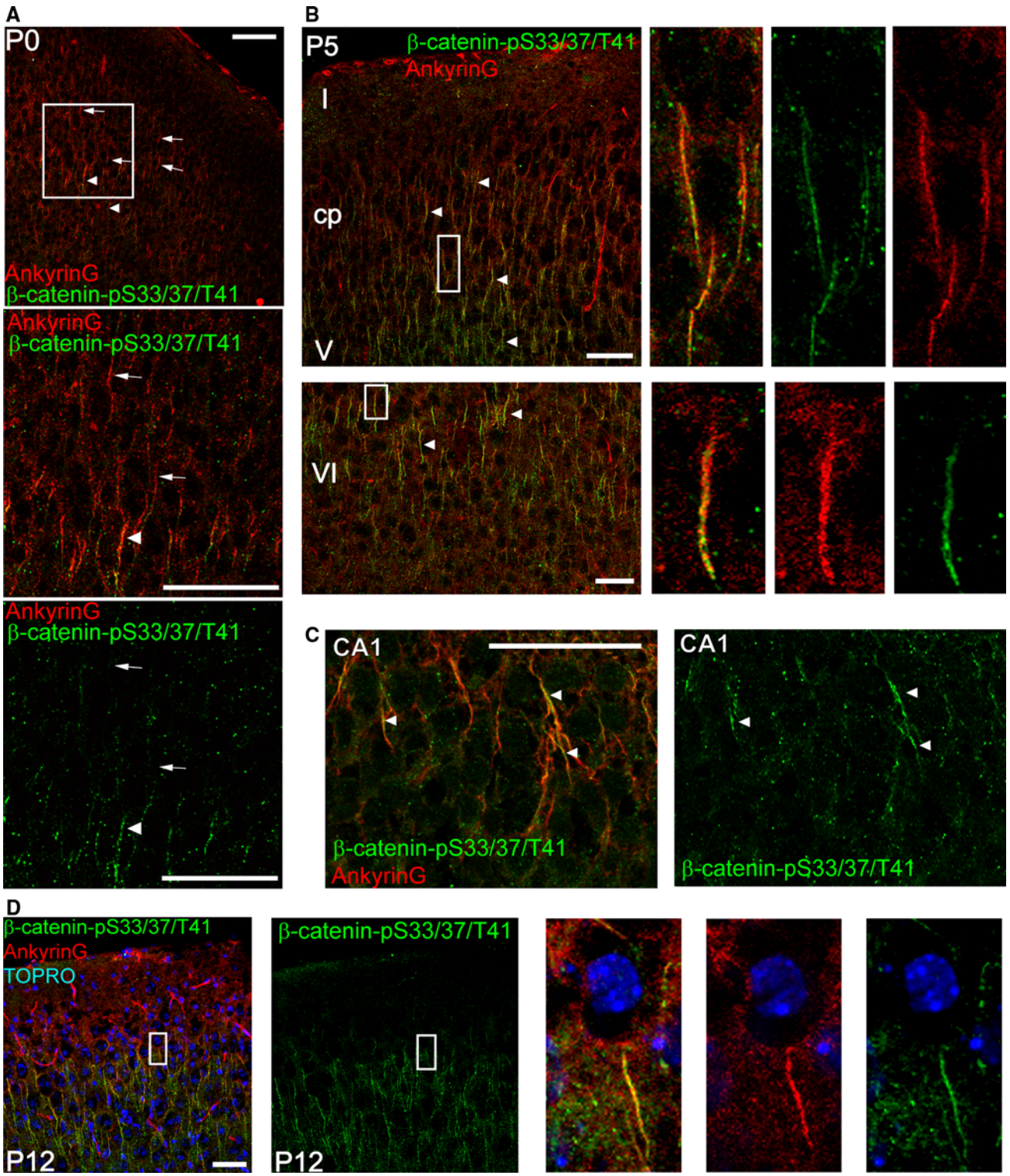

Fig. 2 *β*-catenin-pS33/37/T41 is enriched at the axon initial segment in vivo. **a**, **b** Photomicrographs obtained from sections showing cortical and subcortical layers from P0 (**a**) and P5 (**b**) mice brains. **c** Photomicrographs of the CA1 region of a P5 mouse hippocampus. Sections were stained with anti-ankyrinG (*red*) and anti-*β*-catenin-pS33/37/T41 (*green*) antibodies. **d** Image of cortical section from P12 mouse showing *β*-catenin-pS33/37/T41 and ankyrinG colocalization at the AIS. Nuclei are stained with TOPRO stain. *Arrows* indicate ankyrinG immunolabeled AISs and *arrowheads* overlapping staining of *β*-catenin-pS33/37/T41 and ankyrinG at the AIS. *Scale bar* 50 μm

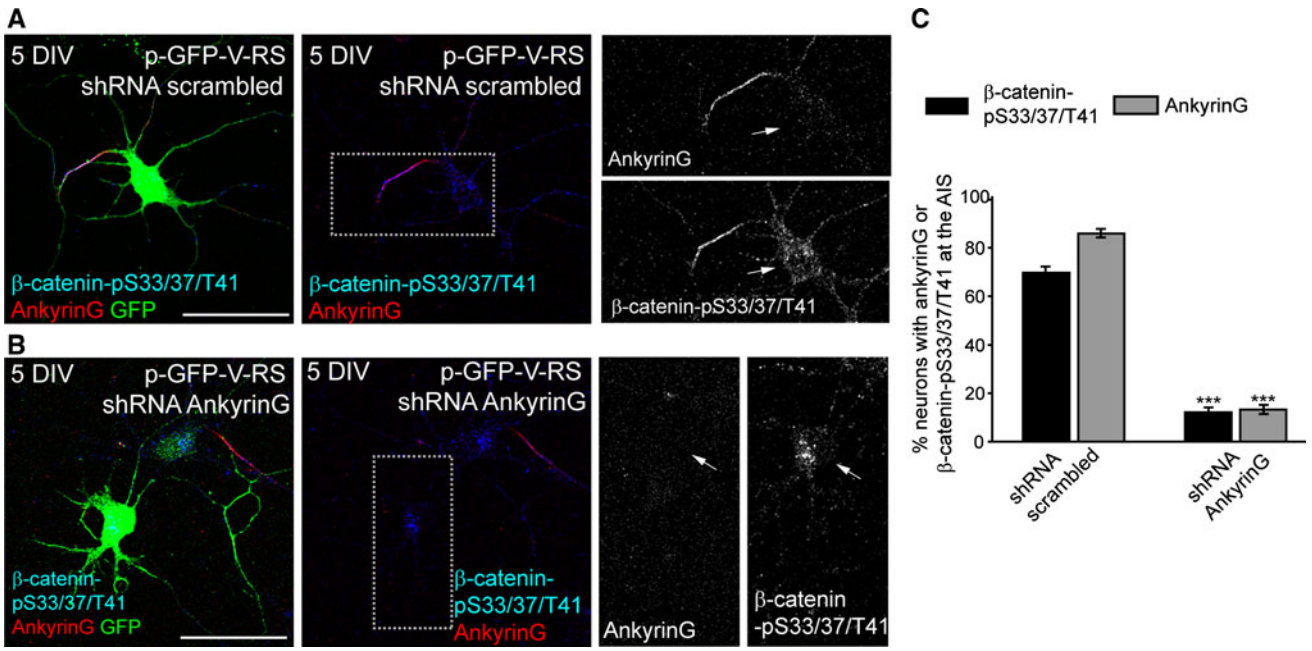

Fig. 3 AnkyrinG expression is necessary to localize β-catenin-pS33/37/T41 to the AIS. **a**, **b** 5-DIV hippocampal neurons nucleofected with GFP plasmids expressing scrambled shRNA (**a**) or ankyrinG shRNA (**b**). Neurons were immunostained with ankyrinG (*red*) and pS33/37T41-β-catenin (*green*) antibodies. Enlarged views of the AIS are shown in *right panels* in gray scale. *Arrows* indicate the position of the soma. **c** The *graph* represents the percentage of neurons with presence of ankyrinG (*gray bars*) or β-catenin-pS33/37/T41 (*black bars*) at the AIS in neurons nucleofected with scrambled or ankyrinG shRNAs. Data represent the mean ± SEM of three independent experiments (50 neurons/experimental condition and experiment). ***$p < 0.001$, *t* test. *Scale bar* 50 μm

We next evaluated whether β-catenin-pS33/37/T41 expression at the AIS was dependent on ankyrinG, which controls the clustering of most AIS proteins [4, 6, 9, 14, 39, 40]. Hippocampal neurons were nucleofected with a scrambled shRNA or with an ankyrinG shRNA [9] and maintained until 5 DIV. Neurons nucleofected with scrambled shRNA had both ankyrinG (85.93 ± 1.61 %) and β-catenin-pS33/37/T41 (69.75 ± 2.08 %) concentrated at the AIS (Fig. 3a, c). In contrast, only 13.19 ± 2.7 % and 12.04 ± 1.17 % of neurons nucleofected with ankyrinG shRNA showed ankyrinG and β-catenin-pS33/37/T41 concentration, respectively (Fig. 3b, c). Moreover, approximately 30 % of neurons nucleofected with ankyrinG shRNA displayed β-catenin-pS33/37/T41 staining concentrated in the soma. Thus, β-catenin-pS33/37/T41 tethering and location at the AIS depends on ankyrinG expression.

To better understand how β-catenin-pS33/37/T41 is anchored at the AIS, we analyzed the involvement of the cytoskeleton in the tethering of β-catenin-pS33/37/T41. As proteins tethered at the AIS, and also microtubules, are insoluble in non-ionic detergents [10, 41], 15-DIV neurons (Fig. 4a) were extracted in 0.5 % TX-100 at 37 °C before fixation. After extraction, voltage-gated sodium channels, ankyrinG, β-catenin-pS33/37/T41 and acetylated-α-tubulin microtubules were found to be concentrated and co-localize at the AIS (Fig. 4b, d). In this context, we have previously shown that changes in microtubule acetylation produced by inhibition of a tubulin deacetylase (HDAC6) impair the tethering of ankyrinG and voltage-gated sodium channels at the AIS [10]. Fifteen-DIV neurons were treated with an HDAC inhibitor, Trichostatin A (TSA), for 48 h, extracted with detergent, and fixed. In these conditions, TSA-treated neurons showed acetylated-α-tubulin staining along the axon, and β-catenin-pS33/37/T41 staining showed a reduction at the AIS, and displayed an extended pattern along the axon (Fig. 4d), indicating that β-catenin-pS33/37/T41 tethering at the AIS depends not only in ankyrinG but also on the properties of AIS microtubules. We then treated 7-DIV neurons for 3 days with a low dose of a microtubule depolymerizing agent, nocodazole (10 nM). In order to evaluate the effects of nocodazole on microtubules, we used an antibody against EB1, a microtubule +TIP protein, also found at the AIS [42, 43]. In control 10-DIV neurons, EB1 was localized throughout the neuron with the characteristics comets, and at the AIS. Nocodazole-induced depolymerization of microtubules reduced EB1 labeling, as well as phospho-β-catenin labeling at the AIS (Fig. 4c). Hence, the changes observed in phospho-β-catenin staining suggest that β-catenin-pS33/37/T41 are related in somehow to changes in AIS microtubule integrity.

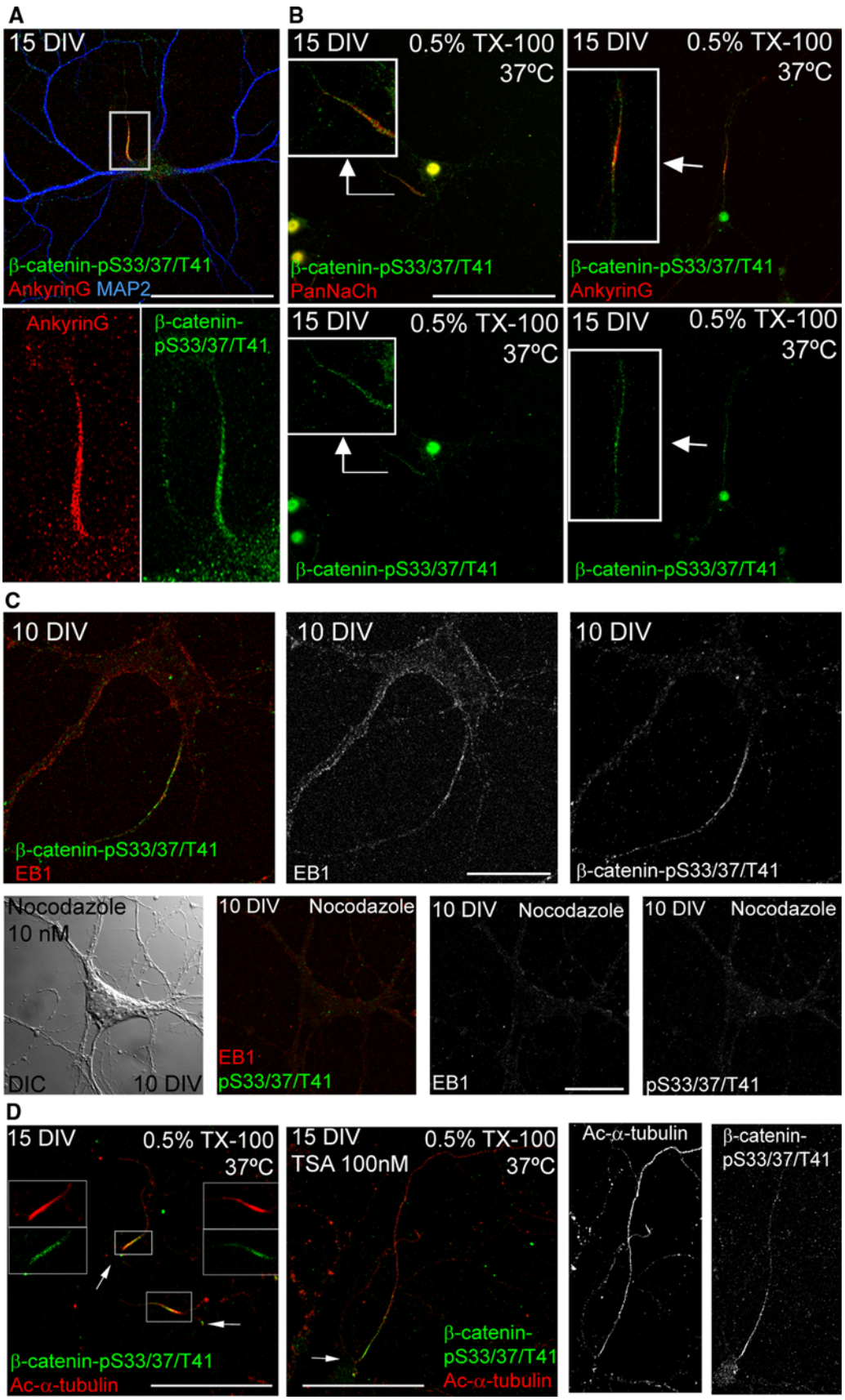
A
15 DIV
β-catenin-pS33/37/T41
AnkyrinG MAP2
AnkyrinG
β-catenin-pS33/37/T41
B
15 DIV 0.5% TX-100 37ºC
β-catenin-pS33/37/T41
PanNaCh
15 DIV 0.5% TX-100 37ºC
β-catenin-pS33/37/T41
AnkyrinG
15 DIV 0.5% TX-100 37ºC
β-catenin-pS33/37/T41
15 DIV 0.5% TX-100 37ºC
β-catenin-pS33/37/T41
C
10 DIV
β-catenin-pS33/37/T41
EB1
10 DIV
EB1
10 DIV
β-catenin-pS33/37/T41
Nocodazole 10 nM
DIC 10 DIV
10 DIV Nocodazole
EB1
pS33/37/T41
10 DIV Nocodazole
EB1
10 DIV Nocodazole
pS33/37/T41
D
15 DIV 0.5% TX-100 37ºC
β-catenin-pS33/37/T41
Ac-α-tubulin
15 DIV 0.5% TX-100 37ºC TSA 100nM
β-catenin-pS33/37/T41
Ac-α-tubulin
Ac-α-tubulin
β-catenin-pS33/37/T41

◀ **Fig. 4** β-catenin-pS33/37/T41 is resistant to detergent extraction at the AIS and its location depends on microtubules. **a** 15-DIV hippocampal neurons stained with antibodies against AnkyrinG (*red*) and β-catenin-pS33/37/T41 (*green*). *Box* indicates the amplified region of the AIS shown in lower panels. **b** 15-DIV hippocampal neurons treated with cytoskeletal buffer (see "Materials and methods" section) for 10 min at 37 °C. After fixation, neurons were stained with β-catenin-pS33/37/T41 and Pan-sodium channel antibodies (*left panels*) or β-catenin-pS33/37/T41 and ankyrinG antibodies (*right panels*). *Insets* show enlarged views of axon initial segments. **c** 10-DIV hippocampal neurons cultured in the absence or presence of nocodazole (10 nM) from 7 to 10 DIV. Neurons were treated with cold methanol (−20 °C) for 5 min before fixation with PFA 4 % and stained with antibodies against EB1 (*red*) and β-catenin-pS33/37/T41 (*green*). A DIC image of nocodazole-treated neurons was obtained to identify the position of the soma. **d** Acetylated-α-tubulin and β-catenin-pS33/37/T41 staining of control or 100 nM TSA-treated 15-DIV neurons extracted with 0.5 % Triton X-100. Note that β-catenin-pS33/37/T41 and acetylated-α-tubulin co-localize at the AIS in control neurons, while β-catenin-pS33/37/T41 is no longer restricted to the AIS and is located along the axon following acetylated-α-tubulin pattern, as previously shown [10]. *Arrows* indicate soma position. *Scale bar* 100 μm in **a**, **b** and **d**, 20 μm in **c**

Inhibition of GSK3 reduces ankyrinG tethering at the AIS and modifies electrophysiological properties

Next, we hypothesized that β-catenin-pS33/37/T41 may have a role in functional maturation after initial formation of the AIS. As β-catenin is phosphorylated at positions 33, 37, and 41 by GSK3, we first analyzed the localization of GSK3 in neurons. While GSK3α/β staining was ubiquitous along the neuron, when neurons were submitted to detergent extraction, interestingly, GSK3α/β staining was detected at the AIS (Fig. 5a). Next, we checked by Western-blot analysis that GSK3 inhibition was able to reduce β-catenin-pS33/37/T41 levels. Short-term GSK3 inhibition, with the previously used GSK3 inhibitor [44], did reduce by 60 % the amount of β-catenin-pS33/37/T41, at the same time that β-catenin levels were increased (Fig. 5b) as expected when GSK3 is inhibited for short times.

In view of these results, we analyzed whether long-term inhibition of GSK3 may modulate AIS protein tethering. Thus, we treated neurons with two other known inhibitors of GSK3, lithium (2.5 or 5 mM) or AR-A014418 (20 μM), a selective GSK3 inhibitor tested against 52 other kinases [45]. Lithium treatment of high-density cultures of cortical neurons, for 24 or 48 h, revealed a 45–65 % reduction in β-catenin phosphorylation (Fig. 6e). Thus, given that β-catenin-pS33/37/T41 enrichment at the AIS starts after 3 DIV (Fig. 1), we treated hippocampal neurons with 2.5 mM LiCl from 4 DIV to 7 DIV (Fig. 6a, b, d). While control neurons show β-catenin-pS33/37/T41 staining at the AIS

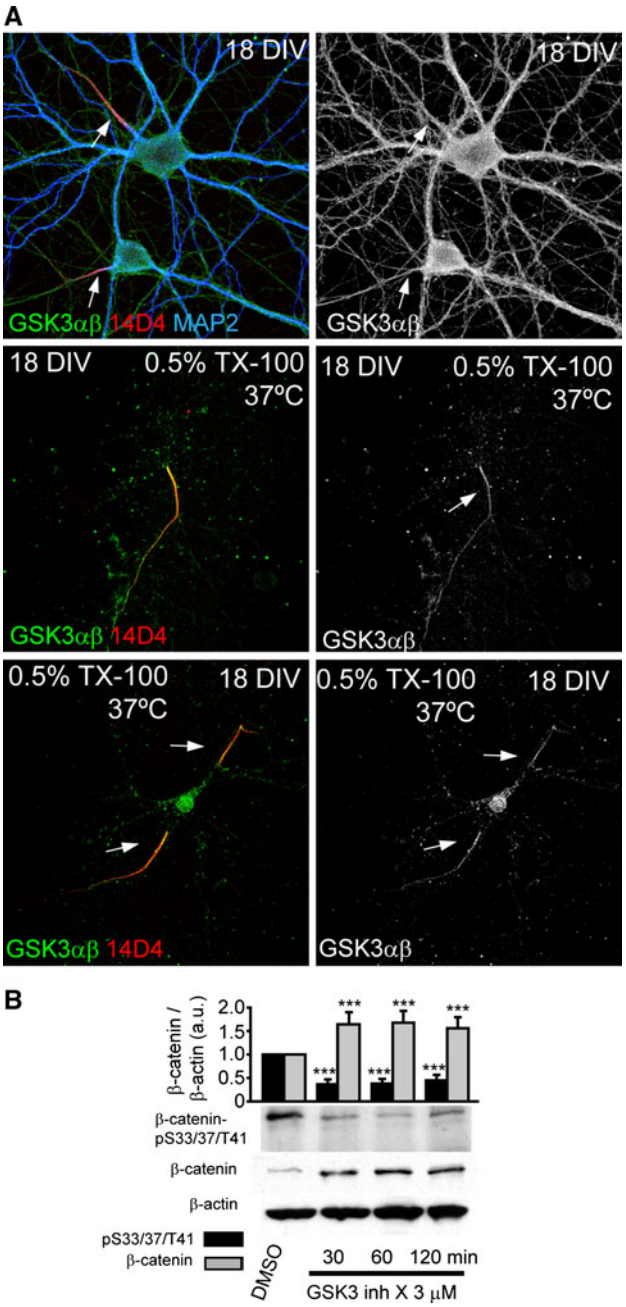

Fig. 5 β-catenin kinase, GSK3, is tethered to the AIS after to detergent extraction. **a** GSK3α/β staining at the AIS of 18-DIV hippocampal neurons after detergent extraction treatment with 0.5 % Triton X-100 for 10 min (*bottom panels*). *Upper panels* show ubiquitous GSK3α/β staining in non-extracted neurons. Extracted and non-extracted neurons were stained with GSK3α/β (*green*), 14D4 (*red*) and MAP2 antibodies (*blue*). *Arrows* indicate the AIS position. **b** Western-blot analysis showing β-catenin and β-catenin-pS33/37/T41 total expression in 2-DIV high-density cortical neurons cultures treated with 3 μM GSK3 inhibitor X for 30, 60, and 120 min. *Graph* represents the mean and SEM of protein expression levels normalized to β-actin in three different experiments. ***$p < 0.001$, *t* test

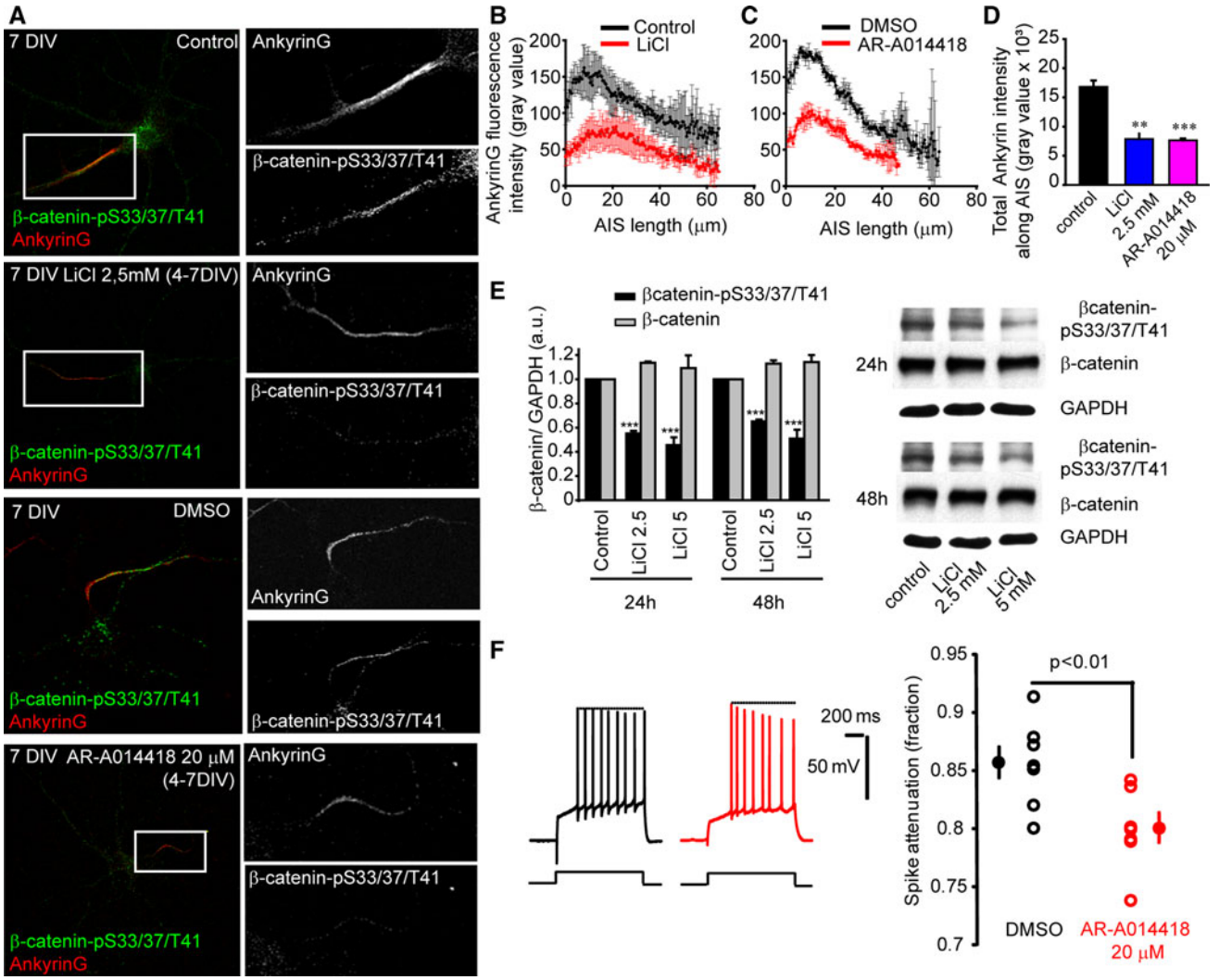

Fig. 6 GSK3 inhibition and *β*-catenin-pS33/37/T41 reduction diminishes ankyrinG clustering at the AIS and modifies action potential characteristics. **a** 7-DIV hippocampal neurons treated with 2.5 mM LiCl or 20 μM AR-A014418 (GSK3 inhibitor) from 4 DIV to 7 DIV and stained for *β*-catenin-pS33/37/T41 (*green*) and ankyrinG (*red*). *Boxes* indicate the amplified AIS region shown on the *right panels* (*gray scale*). **b**, **c** Mean ± SEM fluorescence intensity of ankyrinG along the AIS in control, LiCl, or AR-A014418-treated neurons as shown in **a**. Fluorescence intensity was measured along the AIS every 0.44 μm of 60 neurons from three independent experiments (20 neurons/experimental condition and experiment) using the ImageJ software. **d** Total ankyrinG fluorescence intensity at the AIS of neurons analyzed in **b** and **c**. *Graph* represents the mean ± SEM. $^{**}p < 0.01$; $^{***}p < 0.001$, *t* test. *Scale bar* 50 μm. **e** *β*-catenin and *β*-catenin-pS33/37/T41 expression in control or 2.5 and 5 mM LiCl-treated neurons for 24 and 48 h. *Graph* represents the mean and SEM of protein expression levels normalized to GAPDH levels in three different experiments. $^{***}p < 0.001$, *t* test. **f** Reduced amplitude of the last spike in cultured slices neurons "in vivo" treated with AR-A014418 20 μM. *Left*, representative traces for control (DMSO, *black*) and treated neuron (AR-A014418, red). Note the reduction in the amplitude of the last spike. *Right*, plot of the spike attenuation (i.e., last spike/first spike) in control (DMSO, *black*) and treated (AR-A014418, *red*) neurons. Unpaired *t* test

co-localized with ankyrinG, *β*-catenin-pS33/37/T41 and ankyrinG staining was absent or highly reduced (2.5 fold) at the AIS of LiCl-treated neurons. The same results were obtained from neurons treated with AR-A014418 (20 μM) compared to DMSO (0.1 %)-treated control neurons (Fig. 6a, c, d).

Subsequently, we examined the functional consequences of GSK3 inhibition and diminished *β*-catenin phosphorylation on the electrical properties of hippocampal neurons. Cultured slices were treated for 7 days with the GSK-3 inhibitor AR-A014418 or vehicle (DMSO) and excitability was compared between the two groups. A significant decrease in the last spike amplitude was observed in AR-A014418 treated neurons (ratio of the last to the first spike: 0.80 ± 0.01 vs. 0.86 ± 0.01 in DMSO-treated neurons, $n = 7$, unpaired *t* test $p < 0.01$, Fig. 6f). This larger spike attenuation was further confirmed (0.85 ± 0.01 vs. 0.90 ± 0.02, $p < 0.05$) when the recordings were performed in the presence of M-type potassium and calcium channel blockers (10 μM XE991 and 50 μM cadmium).

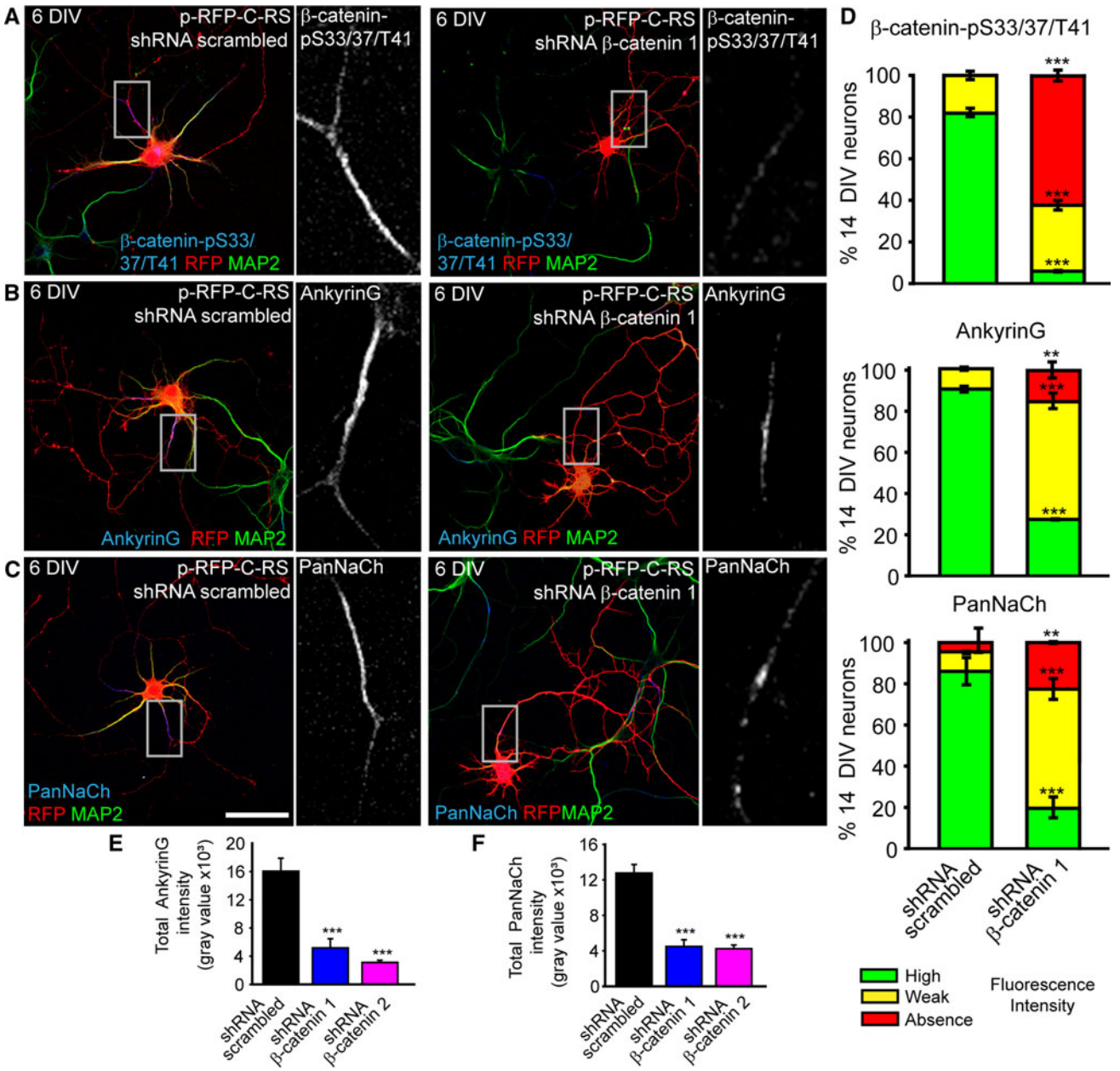

Fig. 7 Suppression of β-catenin-pS33/37/T41 expression by β-catenin interference shRNAs reduces ankyrinG, voltage-gated sodium channels clustering at the AIS. **a–c** 6-DIV hippocampal neurons nucleofected with RFP plasmids expressing scrambled shRNA or β-catenin shRNA. Neurons were stained with antibodies against β-catenin-pS33/37/T41 (**a**), ankyrinG (**b**), and PanNaCh (**c**). Neuronal somatodendritic compartment was identified by MAP2 antibody staining. *Insets* show enlarged views of the indicated axon initial segment (*gray scale*). **d** *Graphs* show the percentage of 14-DIV neurons showing high intensity (*green*), weak intensity (*yellow*) or absence (*red*) of β-catenin-pS33/37/T41, ankyrinG, or sodium channels expression at the AIS of neurons expressing scrambled shRNA or β-catenin shRNA1. Neurons were considered in the weak intensity category when total staining intensity was 50 % or lower than that of control neurons mean. Data represent the mean ± SEM of three independent experiments (100 neurons/experimental condition in each experiment). $***p < 0.001$ and $**p < 0.01$ compared to scrambled shRNA, *t* test. **e**, **f** *Bar graphs* represent the total fluorescence intensity of ankyrinG and PanNaCh staining measured every 0.4 µm along the AIS in 50 neurons/experiment of those quantified in **d**. $***p < 0.001$, *t* test. All images were acquired using the same fluorescence parameters. *Scale bar* 50 µm

Suppression of β-catenin reduces AIS protein tethering and neuronal excitability

To fully understand the role of β-catenin-pS33/37/T41 in AIS maturation, we carried out a second experimental strategy using two shRNAs against β-catenin. After nucleofection, hippocampal neurons were maintained in culture until 6 DIV or 14 DIV (i.e., when the AIS is fully formed). Both β-catenin shRNAs increased the percentage of neurons in which β-catenin-pS33/37/T41 staining was

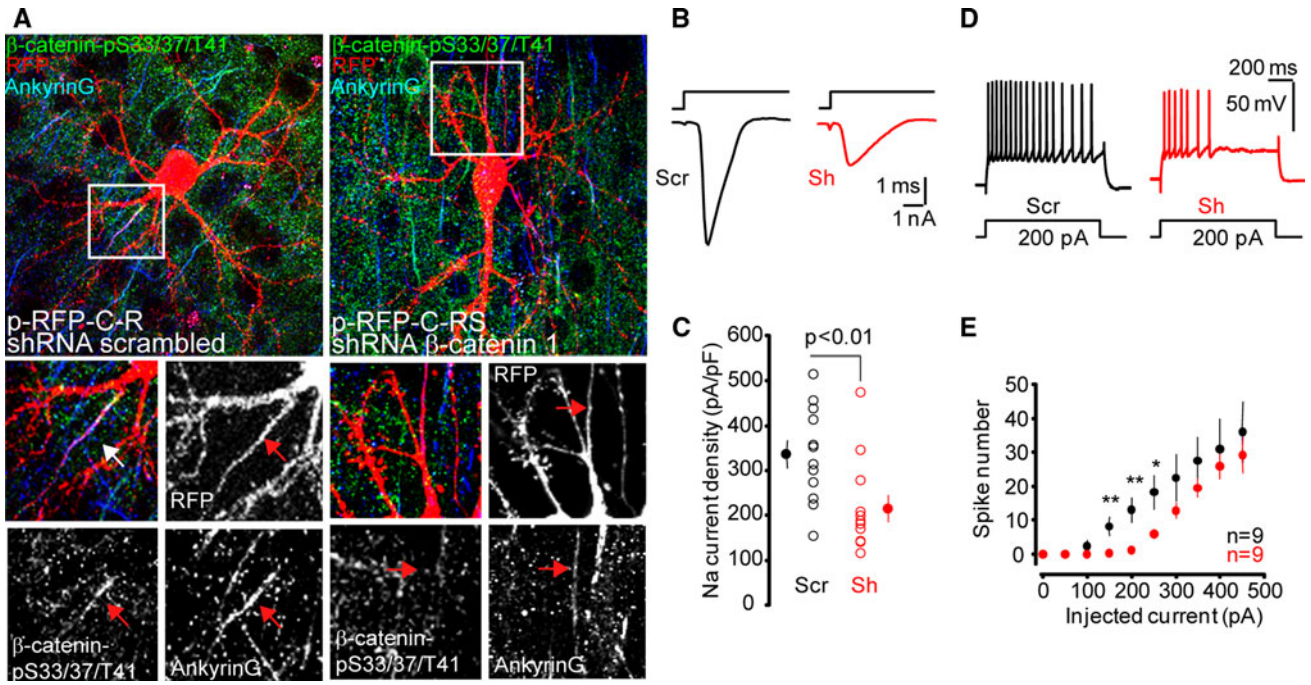

Fig. 8 β-catenin interference diminishes ankyrinG and β-catenin-pS33/37/T41 expression at the AIS, voltage-gated sodium channel current and action potential firing in brain slices. **a** Representative cortical neurons in mice brain slices expressing RFP and scrambled or β-catenin shRNAs. Brain slices were obtained from P8 mice, cultured for 2 days prior to plasmids delivery to neurons by GeneGun. Plasmid expression was allowed for 7 days before electrophysiological recordings and fixation. Slices were stained with antibodies against β-catenin-pS33/37/T41 (*green*) and ankyrinG (*blue*). *Insets* show a magnification of the AIS region. *Arrows* indicate AIS position. Note that in neurons expressing β-catenin interference shRNA, β-catenin-pS33/37/T41 immunoreactivity is absent at the AIS and ankyrinG intensity is reduced compared to scrambled neurons. *Scale bar* 50 μm. **b** Sodium currents measured in L5 pyramidal neurons expressing the β-catenin shRNA 1 plasmid (Sh) or the scrambled shRNA (Scr) were evoked by a depolarizing step from −80 to −20 mV. **c** Plot of the sodium current density for test (Sh) and control (Scr) neurons. Note the significant reduction in the current density (unpaired *t* test). **d** Representative firing profiles for Scr and Sh neurons. **e** Input–output curves for Scr and Sh neurons. Note the significant reduction in excitability for Sh neurons (unpaired *t* test, ** $p < 0.01$, *$p < 0.02$)

absent or reduced (Fig. 7a, d and supplementary Fig. 7). Both β-catenin shRNAs slightly reduced axonal length at 3 DIV without affecting the further axonal elongation, and affected more significantly dendrites development (Supplementary Fig. 8) as previously shown [29]. Fluorescence intensity was measured along the AIS and staining was considered reduced or weak when total fluorescence intensity was 50 % or less than the mean fluorescence measured at control neurons (Fig. 7e, f). β-catenin shRNA1 was more efficient than shRNA2, in agreement with the results shown in supplementary Fig. 1, and their effects increased from 6 DIV to 14 DIV (Supplementary Fig. 7). In 14-DIV neurons, β-catenin-pS33/37/T41 was highly expressed at the AIS in 82 ± 1 % of scrambled shRNA nucleofected neurons and only 18 ± 2 % of neurons showed weak fluorescence intensity (Fig. 7d). In contrast, only 6 ± 1 % of β-catenin shRNA 1 had high-intensity β-catenin-pS33/37/T41 labeling at the AIS (Fig. 7d). In view of our results, we examined the tethering of other proteins (ankyrinG and voltage-gated sodium channel) at the AIS in neurons nucleofected with β-catenin shRNAs (Fig. 7 and Supplementary Fig. 7). Only 27 ± 1 % of neurons nucleofected with β-catenin shRNA 1 exhibited strong tethering of ankyrinG at AISs, compared to 91 ± 1 % of scrambled shRNA-nucleofected neurons (Fig. 7b, d). In these neurons, the average ankyrinG intensity along the AIS was reduced fourfold compared to control neurons (Fig. 7e). In agreement with the reduction in ankyrinG tethering, the expression of sodium channels at the AIS was diminished in 6-DIV and 14-DIV neurons nucleofected with β-catenin shRNAs, exhibiting the same pattern of three clearly different phenotypes (Fig. 7c, d, f, and supplementary Fig. 7).

Hence, we examined the functional consequences of the elimination of β-catenin-pS33/37/T41. Scrambled or β-catenin shRNA 1 plasmids were delivered using GeneGun into cultured brain slices obtained from post-natal day 8 mice and analyzed 9 days later. In this experimental condition, AIS is completely formed at post-natal day 8 before β-catenin suppression. Neurons expressing the scrambled shRNA showed β-catenin-pS33/37/T41 and ankyrinG expression at their AIS, while in neurons expressing the β-catenin shRNA 1 plasmid, β-catenin-pS33/37/T41 expression at the AIS was strongly reduced or

absent and ankyrinG staining was decreased (Fig. 8a). The functional effect of this reduced expression was analyzed using patch-clamp recording. Transfected neurons were identified by their RFP fluorescence. The amplitude of the sodium current evoked by a voltage command from a holding potential of −80 to −20 mV was significantly reduced in L5 pyramidal neurons expressing the β-catenin shRNA 1 plasmid (Fig. 8b). The density of sodium current was 336 ± 31 pA/pF ($n = 12$) in neurons expressing the scrambled shRNA and 215 ± 30 pA/pF ($n = 12$) in neurons expressing the β-catenin shRNA 1 plasmid (unpaired t test, $p < 0.01$; Fig. 8c). We next compared excitability in the two classes of neurons in current clamp by injecting current steps of increasing amplitude. Compared to control neurons (scrambled shRNA), neurons expressing the β-catenin shRNA were found to be less excitable (Fig. 8d). The number of spikes evoked by 150, 200, or 250 pA was significantly reduced in neurons expressing β-catenin shRNA (Fig. 8e).

Thus, the fact that GSK3 inhibition, which stabilizes β-catenin levels, and β-catenin levels reduction with interference RNAs, results in a reduction of AIS proteins tethering suggest that β-catenin-pS33/37/T41 has a role in the functional maturation and maintenance of the AIS. Further experiments will be necessary to understand the complex role of GSK3 and β-catenin at the AIS.

Discussion

The underlying cellular mechanisms that regulate ion channel expression and maintenance at the membrane of the AIS, and therefore action potential regulation and excitability, are only beginning to be studied. It is generally recognized that ankyrinG is an important protein for the organization and assembly of the AIS [6, 14, 46, 47] and its tethering at the AIS is necessary for the concentration of other AIS proteins. However, little is known about the mechanisms that modulate and maintain the expression of proteins at the AIS.

Our results show for the first time the localization of GSK3 at the AIS and its role in the functional maturation and maintenance of the AIS. Moreover, GSK3 phosphorylated β-catenin is also tethered at the AIS and depends on ankyrinG expression. Both pharmacological inhibition of its phosphorylation by GSK3 or reduction of β-catenin levels diminished ankyrinG tethering at the AIS and the functional expression of voltage-gated sodium channels. These data bring a new insight into AIS maturation and is particularly relevant to neurodevelopment given the importance of this neuronal compartment in action potential initiation and in the control of polarized axonal traffic. Moreover, our data may be related to schizophrenia, a mental disease with a neurodevelopmental origin, as post-mortem schizophrenic patients' brains show reduced GSK3 levels [48], abnormal GSK3 activity, and also a reduction of ankyrinG tethering at the AIS [49].

β-catenin-pS33/37/T41 shows a progressive enrichment at the AIS during development, reflecting the establishment of barriers to membrane diffusion and cytoplasmic traffic. A higher percentage of neurons with β-catenin-pS33/37/T41 tethering at the AIS was attained after 7 DIV, when the AIS forms a fully assembled membrane diffusion barrier [50]. In fact, the membrane diffusion barrier is not yet functional at 4 DIV, when only a small percentage of neurons show β-catenin-pS33/37/T41 tethering at the AIS. Moreover, the cytoplasmic traffic barrier of the AIS starts to appear at 3 DIV and is complete at 5 DIV [13] when at least 70 % of neurons show β-catenin-pS33/37/T41 tethering at the AIS.

Our data suggest that β-catenin-pS33/37/T41 is not necessary for the initial development of the AIS, but its enrichment plays a role in the maturation of AIS functions, modulating neuronal excitability and voltage-gated sodium currents. Previous works have shown that GSK3 is involved in LTP and LTD regulation [51–53], and β-catenin participates in the regulation of neuronal activity [54]. Regarding a possible function of β-catenin-pS33/37/T41 in action potential generation, the inhibition of GSK3 or β-catenin suppression decreased excitability in neurons from cultured brain slices. Although no interaction between voltage-gated sodium channels and β-catenin has been described, our data show that the loss of β-catenin-pS33/37/T41 is related to neuronal excitability by reducing voltage-gated sodium currents. While not excluding parallel transcriptional effects and since the decreased neuronal excitability observed in our study occurs independently of β-catenin levels, our results suggest that this effect is mediated by β-catenin-pS33/37/T41 rather than β-catenin levels. Thus, sodium current reduction is most probably due to diminished ankyrinG tethering at the AIS and the loss of AIS integrity when β-catenin-pS33/37/T41 is absent. In fact, AIS integrity is also lost in ankyrinG knockout mice [3], and it has been proposed that AIS integrity could be a critical determinant of the threshold and waveform of action potentials [55]. An interaction between β-catenin and large-conductance Ca^{2+}-activated K^+ channels has been reported [34]. In addition, GSK3 participates in the regulation of the KCNQ2 potassium channels [56]. However, neither pharmacological inhibition of KCNQ2 nor voltage-gated calcium channel block using cadmium change the spike attenuation induced by GSK3 inhibition.

In the last decade, many reports have focused on understanding how different phosphorylation sites on β-catenin can define its binding interactions and therefore

different sub-cellular fates [21, 57]. In this context, it is also necessary to take into account different conformational modifications, such C-terminal region folding, proposed to prevent β-catenin degradation [58]. Tyrosine phosphorylation of β-catenin disrupts its interaction with N-cadherin and leads to its mobilization from membranes [59] to the nucleus or neuronal cytoskeleton [60]. On the other hand, while N-terminally unphosphorylated β-catenin (S33/S37/T41), located in the nucleus, seems to better correlate with Wnt signaling functions [61, 62], N-terminally GSK3 phosphorylated (β-catenin-pS33/37/T41) and ubiquitinated β-catenin is thought to be targeted for degradation at the proteasome [63]. Our results describe a new GSK3-phosphorylated β-catenin pool localized at the AIS, which participates in the AIS functions and is not immediately targeted to the proteasome.

Given the ubiquitous expression of GSK3, the stability of this pool of β-catenin-pS33/37/T41 at the AIS may be the consequence of the absence of APC (Supplementary Fig. 4), a critical component for β-catenin destruction [64]. In fact, APC co-clusters with stabilized non-phosphorylated β-catenin at neurite tips [33]. On the other hand, β-catenin is resistant to proteasome degradation when phosphorylated by CK2 [65], which is expressed at the AIS and regulates some of its properties [9, 66]. Finally, unidentified chaperones at the AIS may serve to protect β-catenin-pS33/37/T41 from degradation.

It has been described that disruption of the AIS actin cytoskeleton generates a reduction in the rate-of-rise of axonal action potentials, estimated as being due to the loss of approximately one-third of the sodium channels from the AIS [1]. Indeed, sustained inhibition of GSK3 by LiCl or a GSK3 selective inhibitor during establishment of the diffusion barrier (4–7 DIV) causes the loss of β-catenin-pS33/37/T41 and ankyrinG concentration at the AIS and a significant decrease in spike amplitude. This is even more significant when β-catenin levels are reduced and sodium current amplitude and the number of action potentials are diminished. Thus, β-catenin-pS33/37/T41 plays an important role in the reinforcement of the AIS.

Other studies have suggested a potential function of β-catenin-pS33/37/T41 in microtubule anchoring and centrosome maturation in epithelial cells [26]. In this sense, we have found that β-catenin phosphorylated by GSK3 is colocalized with microtubules in neurites in stage 2 and 3 hippocampal neurons. In more mature neurons, the AIS β-catenin-pS33/37/T41 pool is resistant to detergent extraction and co-localizes with detergent-resistant acetylated-α-tubulin microtubules, like other AIS proteins [10]. Microtubules at the AIS have distinct properties from those in dendrites [12, 43] and are highly enriched in more stable acetylated and detyrosinated microtubules. Changes in post-translational modifications of tubulin, such as acetylation, can disturb protein tethering at the AIS [9, 10], and such is the case for β-catenin-pS33/37/T41, which after tubulin hyper-acetylation was localized all along the axon together with acetylated-α-tubulin. This absence of β-catenin-pS33/37/T41 enrichment is consistent with the loss of ankyrinG and sodium channel concentration at the AIS after disruption of its cytoskeleton [10]. Furthermore, nocodazole-induced depolymerization abolished β-catenin-pS33/37/T41 clustering in the AIS in our experiments, and also that of another AIS-tethered protein, EB1 [42, 43], suggesting a possible relationship with AIS cytoskeleton or a regulating function of β-catenin-pS33/37/T41. In fact, β-catenin suppression in brain slices once the AIS is formed alters the pattern of action potential generation and ankyrinG tethering.

In summary, we have found a new pool of β-catenin-pS33/37/T41 and its kinase, GSK3, at the AIS that regulate AIS maturation and modulate neuronal excitability through regulation of ankyrinG tethering, which in turn is responsible for the anchoring of sodium channels. The present findings represent an advance for the understanding of the molecular mechanisms underlying neuronal action potential generation. They raise the hypothesis that β-catenin phosphorylation and GSK3 activity at the AIS may be involved in mental diseases related to neuronal development and excitability, such as epilepsy, schizophrenia, or bipolar disorder. In fact, reduced levels of β-catenin expression and altered GSK3 function have been detected in schizophrenia patients [67]. Further experiments will be necessary to completely understand how GSK3 and phosphorylated β-catenin participates in AIS function and development.

Acknowledgments The authors would like to acknowledge Hector Diez, Sylvain Rama, Alfonso Araque, and Michael Seagar for their advice and critical reading of the manuscript. This work was supported by grants SAF2009-12249-C02-02 and SAF2009-12249-C02-01 from the Ministerio de Ciencia e Innovacion (Spain), by the Centro de Investigación Biomédica en Red de Enfermedades Neurodegenerativas (CIBERNED, Spain), INSERM and Agence National de la Recherche (EXCION, EPISOM). Mónica Tapia is supported by a CSIC-JAE fellowship.

References

1. Kole MH et al (2008) Action potential generation requires a high sodium channel density in the axon initial segment. Nat Neurosci 11:178–186
2. Kole MH, Letzkus JJ, Stuart GJ (2007) Axon initial segment Kv1 channels control axonal action potential waveform and synaptic efficacy. Neuron 55:633–647
3. Ango F et al (2004) Ankyrin-based subcellular gradient of neurofascin, an immunoglobulin family protein, directs GABAergic innervation at purkinje axon initial segment. Cell 119:257–272
4. Garrido JJ et al (2003) A targeting motif involved in sodium channel clustering at the axonal initial segment. Science 300: 2091–2094

5. Ogawa Y et al (2008) Postsynaptic density-93 clusters Kv1 channels at axon initial segments independently of Caspr2. J Neurosci 28:5731–5739
6. Zhou D et al (1998) AnkyrinG is required for clustering of voltage-gated Na channels at axon initial segments and for normal action potential firing. J Cell Biol 143:1295–1304
7. Nakada C et al (2003) Accumulation of anchored proteins forms membrane diffusion barriers during neuronal polarization. Nat Cell Biol 5:626–632
8. Palay SL, Sotelo C, Peters A, Orkand PM (1968) The axon hillock and the initial segment. J Cell Biol 38:193–201
9. Sanchez-Ponce D, Munoz A, Garrido JJ (2011) Casein kinase 2 and microtubules control axon initial segment formation. Mol Cell Neurosci 46:222–234
10. Tapia M, Wandosell F, Garrido JJ (2010) Impaired function of HDAC6 slows down axonal growth and interferes with axon initial segment development. PLoS One 5:e12908
11. Winckler B, Forscher P, Mellman I (1999) A diffusion barrier maintains distribution of membrane proteins in polarized neurons. Nature 397:698–701
12. Konishi Y, Setou M (2009) Tubulin tyrosination navigates the kinesin-1 motor domain to axons. Nat Neurosci 12:559–567
13. Song AH et al (2009) A selective filter for cytoplasmic transport at the axon initial segment. Cell 136:1148–1160
14. Hedstrom KL, Ogawa Y, Rasband MN (2008) AnkyrinG is required for maintenance of the axon initial segment and neuronal polarity. J Cell Biol 183:635–640
15. Sobotzik JM et al (2009) AnkyrinG is required to maintain axo-dendritic polarity in vivo. Proc Natl Acad Sci USA 106:17564–17569
16. Ciani L, Salinas PC (2007) c-Jun N-terminal kinase (JNK) cooperates with Gsk3beta to regulate Dishevelled-mediated microtubule stability. BMC Cell Biol 8:27
17. Jope RS, Johnson GV (2004) The glamour and gloom of glycogen synthase kinase-3. Trends Biochem Sci 29:95–102
18. Morfini G et al (2004) A novel CDK5-dependent pathway for regulating GSK3 activity and kinesin-driven motility in neurons. EMBO J 23:2235–2245
19. Zhou FQ, Zhou J, Dedhar S, Wu YH, Snider WD (2004) NGF-induced axon growth is mediated by localized inactivation of GSK-3beta and functions of the microtubule plus end binding protein APC. Neuron 42:897–912
20. Tyagarajan SK et al (2011) Regulation of GABAergic synapse formation and plasticity by GSK3beta-dependent phosphorylation of gephyrin. Proc Natl Acad Sci USA 108:379–384
21. Gottardi CJ, Gumbiner BM (2004) Distinct molecular forms of beta-catenin are targeted to adhesive or transcriptional complexes. J Cell Biol 167:339–349
22. Liu C et al (2002) Control of beta-catenin phosphorylation/degradation by a dual-kinase mechanism. Cell 108:837–847
23. Hart M et al (1999) The F-box protein beta-TrCP associates with phosphorylated beta-catenin and regulates its activity in the cell. Curr Biol 9:207–210
24. Faux MC, Coates JL, Kershaw NJ, Layton MJ, Burgess AW (2010) Independent interactions of phosphorylated beta-catenin with E-cadherin at cell-cell contacts and APC at cell protrusions. PLoS One 5:e14127
25. Maher MT, Mo R, Flozak AS, Peled ON, Gottardi CJ (2010) Beta-catenin phosphorylated at serine 45 is spatially uncoupled from beta-catenin phosphorylated in the GSK3 domain: implications for signaling. PLoS One 5:e10184
26. Huang P, Senga T, Hamaguchi M (2007) A novel role of phospho-beta-catenin in microtubule regrowth at centrosome. Oncogene 26:4357–4371
27. Shaw RM et al (2007) Microtubule plus-end-tracking proteins target gap junctions directly from the cell interior to adherens junctions. Cell 128:547–560
28. Ligon LA, Karki S, Tokito M, Holzbaur EL (2001) Dynein binds to beta-catenin and may tether microtubules at adherens junctions. Nat Cell Biol 3:913–917
29. Yu X, Malenka RC (2003) Beta-catenin is critical for dendritic morphogenesis. Nat Neurosci 6:1169–1177
30. Yu X, Malenka RC (2004) Multiple functions for the cadherin/catenin complex during neuronal development. Neuropharmacology 47:779–786
31. Haegel H et al (1995) Lack of beta-catenin affects mouse development at gastrulation. Development 121:3529–3537
32. Campos VE, Du M, Li Y (2004) Increased seizure susceptibility and cortical malformation in beta-catenin mutant mice. Biochem Biophys Res Commun 320:606–614
33. Votin V, Nelson WJ, Barth AI (2005) Neurite outgrowth involves adenomatous polyposis coli protein and beta-catenin. J Cell Sci 118:5699–5708
34. Lesage F, Hibino H, Hudspeth AJ (2004) Association of beta-catenin with the alpha-subunit of neuronal large-conductance Ca^{2+}-activated K^{+} channels. Proc Natl Acad Sci USA 101:671–675
35. Kaech S, Banker G (2006) Culturing hippocampal neurons. Nat Protoc 1:2406–2415
36. Debanne D et al (2008) Paired-recordings from synaptically coupled cortical and hippocampal neurons in acute and cultured brain slices. Nat Protoc 3:1559–1568
37. Chilov D et al (2011) Phosphorylated beta-catenin localizes to centrosomes of neuronal progenitors and is required for cell polarity and neurogenesis in developing midbrain. Dev Biol 357:259–268
38. Sanchez-Ponce D, Tapia M, Munoz A, Garrido JJ (2008) New role of IKK alpha/beta phosphorylated I kappa B alpha in axon outgrowth and axon initial segment development. Mol Cell Neurosci 37:832–844
39. Pan Z et al (2006) A common ankyrin-G-based mechanism retains KCNQ and NaV channels at electrically active domains of the axon. J Neurosci 26:2599–2613
40. Rasband MN (2010) The axon initial segment and the maintenance of neuronal polarity. Nat Rev Neurosci 11:552–562
41. Winckler B, Mellman I (1999) Neuronal polarity: controlling the sorting and diffusion of membrane components. Neuron 23:637–640
42. Leterrier C et al (2011) End-binding proteins EB3 and EB1 link microtubules to ankyrin G in the axon initial segment. Proc Natl Acad Sci USA 108(21):8826–8831
43. Nakata T, Hirokawa N (2003) Microtubules provide directional cues for polarized axonal transport through interaction with kinesin motor head. J Cell Biol 162:1045–1055
44. Kim WY et al (2006) Essential roles for GSK-3s and GSK-3-primed substrates in neurotrophin-induced and hippocampal axon growth. Neuron 52:981–996
45. Bhat R et al (2003) Structural insights and biological effects of glycogen synthase kinase 3-specific inhibitor AR-A014418. J Biol Chem 278:45937–45945
46. Hedstrom KL et al (2007) Neurofascin assembles a specialized extracellular matrix at the axon initial segment. J Cell Biol 178:875–886
47. Jenkins SM, Bennett V (2001) Ankyrin-G coordinates assembly of the spectrin-based membrane skeleton, voltage-gated sodium channels, and L1 CAMs at Purkinje neuron initial segments. J Cell Biol 155:739–746
48. Nadri C, Dean B, Scarr E, Agam G (2004) GSK-3 parameters in postmortem frontal cortex and hippocampus of schizophrenic patients. Schizophr Res 71:377–382
49. Cruz DA, Weaver CL, Lovallo EM, Melchitzky DS, Lewis DA (2009) Selective alterations in postsynaptic markers of chandelier cell inputs to cortical pyramidal neurons in subjects with schizophrenia. Neuropsychopharmacology 34:2112–2124

50. Brachet A et al (2010) Ankyrin G restricts ion channel diffusion at the axonal initial segment before the establishment of the diffusion barrier. J Cell Biol 191:383–395
51. Peineau S et al (2009) A systematic investigation of the protein kinases involved in NMDA receptor-dependent LTD: evidence for a role of GSK-3 but not other serine/threonine kinases. Mol Brain 2:22
52. Peineau S et al (2007) LTP inhibits LTD in the hippocampus via regulation of GSK3beta. Neuron 53:703–717
53. Zhu LQ et al (2007) Activation of glycogen synthase kinase-3 inhibits long-term potentiation with synapse-associated impairments. J Neurosci 27:12211–12220
54. Peng YR et al (2009) Coordinated changes in dendritic arborization and synaptic strength during neural circuit development. Neuron 61:71–84
55. Zonta B et al (2011) A critical role for neurofascin in regulating action potential initiation through maintenance of the axon initial segment. Neuron 69:945–956
56. Kapfhamer D et al (2010) Protein phosphatase 2a and glycogen synthase kinase 3 signaling modulate prepulse inhibition of the acoustic startle response by altering cortical M-Type potassium channel activity. J Neurosci 30:8830–8840
57. Daugherty RL, Gottardi CJ (2007) Phospho-regulation of beta-catenin adhesion and signaling functions. Physiology (Bethesda) 22:303–309
58. Mo R et al (2009) The terminal region of beta-catenin promotes stability by shielding the Armadillo repeats from the axin-scaffold destruction complex. J Biol Chem 284:28222–28231
59. Roura S, Miravet S, Piedra J, Garcia de Herreros A, Dunach M (1999) Regulation of E-cadherin/catenin association by tyrosine phosphorylation. J Biol Chem 274:36734-36740
60. David MD et al (2008) Signalling by neurotrophins and hepatocyte growth factor regulates axon morphogenesis by differential beta-catenin phosphorylation. J Cell Sci 121:2718–2730
61. Staal FJ, Noort Mv M, Strous GJ, Clevers HC (2002) Wnt signals are transmitted through N-terminally dephosphorylated beta-catenin. EMBO Rep 3:63-68
62. Hendriksen J et al (2008) Plasma membrane recruitment of dephosphorylated {beta}-catenin upon activation of the Wnt pathway. J Cell Sci 121:1793–1802
63. Winston JT et al (1999) The SCFbeta-TRCP-ubiquitin ligase complex associates specifically with phosphorylated destruction motifs in IkappaBalpha and beta-catenin and stimulates IkappaBalpha ubiquitination in vitro. Genes Dev 13:270–283
64. Su Y et al (2008) APC is essential for targeting phosphorylated beta-catenin to the SCFbeta-TrCP ubiquitin ligase. Mol Cell 32:652–661
65. Song DH et al (2003) CK2 phosphorylation of the armadillo repeat region of beta-catenin potentiates Wnt signaling. J Biol Chem 278:24018–24025
66. Brechet A et al (2008) Protein kinase CK2 contributes to the organization of sodium channels in axonal membranes by regulating their interactions with ankyrin G. J Cell Biol 183:1101–1114
67. Lovestone S, Killick R, Di Forti M, Murray R (2007) Schizophrenia as a GSK-3 dysregulation disorder. Trends Neurosci 30:142–149